Earthq Eng & Eng Vib (2018) 17: 149-163 **DOI**: https://doi.org/10.1007/s11803-018-0431-3

Derivation of energy-based base shear force coefficient considering hysteretic behavior and P-delta effects

Taner Ucar[1†] and Onur Merter[2‡]

1. *Department of Architecture, Dokuz Eylul University, Izmir, Turkey*

2. .*Department of Civil Engineering, Dokuz Eylul University, Izmir, Turkey*

Abstract: A modified energy-balance equation accounting for P-delta effects and hysteretic behavior of reinforced concrete members is derived. Reduced hysteretic properties of structural components due to combined stiffness and strength degradation and pinching effects, and hysteretic damping are taken into account in a simple manner by utilizing plastic energy and seismic input energy modification factors. Having a pre-selected yield mechanism, energy balance of structure in inelastic range is considered. P-delta effects are included in derived equation by adding the external work of gravity loads to the work of equivalent inertia forces and equating the total external work to the modified plastic energy. Earthquake energy input to multi degree of freedom (MDOF) system is approximated by using the modal energy-decomposition. Energy-based base shear coefficients are verified by means of both pushover analysis and nonlinear time history (NLTH) analysis of several RC frames having different number of stories. NLTH analyses of frames are performed by using the time histories of ten scaled ground motions compatible with elastic design acceleration spectrum and fulfilling duration/amplitude related requirements of Turkish Seismic Design Code. The observed correlation between energy-based base shear force coefficients and the average base shear force coefficients of NLTH analyses provides a reasonable confidence in estimation of nonlinear base shear force capacity of frames by using the derived equation.

Keywords: energy-based base shear force coefficient; reduced hysteretic behavior; P-delta effect; pushover analysis; nonlinear time history analysis

1 Introduction

The general trend in determination of base shear force for each lateral direction in seismic codes is typically based on elastic response spectrum analysis. Natural vibration period is the basic parameter in strength-based seismic design since it specifies the spectral acceleration and thus the elastic base shear force. It is impractical yet not economical to design structures to withstand seldom major earthquakes within their elastic limits. Consequently, the linear elastic base shear force is reduced by employing response reduction factors to account for the ductility capacity of the system and the inherent overstrength for design purposes and the reduced seismic forces are distributed laterally through the total height of structure. However, it is well recognized that structures (particularly with large R values) designed in accordance with current seismic design codes are exposed to large nonlinear deformations during severe earthquakes.

Correspondence to: Taner Ucar, Department of Architecture, Dokuz Eylul University, Izmir, Turkey
Tel: +90-232-301 8410; Fax: +90-232-453 2986
E-mail: taner.ucar@deu.edu.tr
[†]Assistant Professor; [‡]PhD

Received October 25, 2016; **Accepted** May 9, 2017

Structural displacements due to seismic actions are the primary cause for the damage in structures subjected to ground motions. Therefore, it seems rational to consider the displacements at the beginning of the design process rather than forces. In this regard, the conventional force-based design methods are insufficient since structural damage states can better be represented by deformation, rather than by strength. Recently, alternative and more realistic design methodologies based more on member deformation capacity, such as displacement-based design based on performance-based design, have become popular with a better understanding of nonlinear structural response. However, the level of earthquake induced damage does not only depend on structural deformations but also on response characteristics obtained from the time history of ground motions (Kim *et al*., 2004; Choi and Kim, 2006; Acun and Sucuoğlu, 2010; Alıcı and Sucuoğlu, 2016).

Energy-based design methods deal directly with hysteretic energy as a main parameter in design, provide a better estimation on inelastic response of structures and control of distribution of the structural damage and energy dissipation mechanism. In this manner they offer more comprehensive solutions for design. It is quite important to consider the inelastic seismic response of structures directly in seismic design procedure to achieve the primary goal of energy-based design methodologies

(Chao *et al*., 2007). Since the basic concepts of energy-based design was originally demonstrated by Housner (1956), a great deal of effort has been devoted to energy concepts (Akiyama, 1985; Uang and Bertero, 1990; Fajfar and Vidic, 1994; Decanini and Mollaioli, 1998; Akbas *et al*., 2001; Chou and Uang, 2003; Park and Eom, 2006; Kalkan and Kunnath, 2008; Leelataviwat *et al*., 2009; Benavent-Climent *et al*., 2010; Lopez-Almansa *et al*., 2013; Wang *et al*., 2015; Ke *et al*., 2016). The energy concept seems the best way to point out the inelastic response of structures subjected to major earthquake excitations (Okur and Erberik, 2012).

In energy-based procedures, the effect of earthquake ground motion is interpreted as seismic energy input to a structure and the design is entirely achieved by providing an adequate dissipation capacity to structural members to dissipate the imposed energy input. Among the specific types of energy, the input energy, i.e. the energy demand, is a stable parameter in structural response and there have been many attempts on consistent prediction of input energy (Housner, 1956; Akiyama, 1985; Uang and Bertero, 1990; Decanini and Mollaioli, 1998; Benavent-Climent *et al*., 2002; Benavent-Climent *et al*., 2010; Tselentis *et al*., 2010; Okur and Erberik, 2012; Dindar *et al*., 2015; Alıcı and Sucuoğlu, 2016). The earthquake energy input to a structure is partly dissipated by damping and through inelastic deformations. The design criterion in energy-based procedures is based on the comparison of earthquake energy input and the energy dissipation capacity of structures. In this regard, the fundamental concepts of energy balance are widely used.

When ductile structures exhibit large inelastic deformations, the destabilising influence of gravitational loads, i.e. P-delta effects, may become significant while P-delta effect is usually not taken into consideration when deformations are within the elastic range. In such a situation, gravitational loads induce a negative slope in the inelastic region of load-displacement curve and they amplify the earthquake induced large inelastic deformations (Adam and Jager, 2011, 2012). The tendency for the displacement to increase indicates the reduction in stiffness of the structure in the inelastic range due to inclusion of P-delta effect (Fenwick *et al*., 1992). P-delta effect corresponds to a potential energy release in the gravitational field and reduces lateral strength of the structure (Akiyama, 2002). Although P-delta effect and its possible influence on both static and dynamic responses of structures has been widely studied, very limited studies account for the effect of P-delta in displacement-based design (Asimakopoulos *et al*., 2007; Pettinga and Priestley, 2007, 2008) while hardly any study existing in scientific literature includes P-delta effect in energy-based design.

Since the inelastic phase of the structure is considered in energy-based procedures, the influence of P-delta effects associated with large lateral displacements may be of prime importance. However, this fact is not taken into consideration, the additional lateral forces due to gravitational loads are not included in design and the energy equilibrium of structures is achieved in a lower base shear. In this study, a more realistic ultimate base shear force coefficient considering P-delta effects is derived by using the input energy from the design pseudo-acceleration spectrum of Turkish Seismic Design Code (TSDC, 2007), a desirable and predictable yield mechanism, and an ultimate target drift. Having pre-targeted the yield mechanism, the derived base shear force accounts for P-delta effects and considers the energy balance of the structure in its inelastic range of response and the reduced hysteretic behavior of reinforced concrete (RC) members. Energy-based base shear force coefficients are verified by means of pushover and NLTH analyses of several RC frames. A very good correlation between energy-based base shear force coefficients and the average base shear force coefficients of NLTH is observed.

2 Modified energy balance concept

Like many other fundamental parameters of structural dynamics, energy related concepts are first formulated based on single degree of freedom (SDOF) system. The seismic response of an inelastic lumped-mass SDOF system subjected to an horizontal earthquake excitation is governed by the following general equation of motion (Chopra, 1995):

$$m\cdot\ddot{u}+c\cdot\dot{u}+f_{\mathrm{s}}(u)=-m\cdot\ddot{u}_{\mathrm{g}}(t) \tag{1}$$

where u is the relative displacement of the system with respect to ground, m is the mass, c is the damping coefficient, $f_{\mathrm{s}}(u)$ is the restoring force for nonlinear system and $\ddot{u}_{\mathrm{g}}(t)$ is the ground acceleration. Energy response parameters of an inelastic SDOF system may be expressed by integrating Eq. (1) over the relative displacement as indicated in Eq. (2):

$$\int_0^{u(t)} m\cdot\ddot{u}\,\mathrm{d}u+\int_0^{u(t)} c\cdot\dot{u}\,\mathrm{d}u+\int_0^{u(t)} f_{\mathrm{s}}(u)\,\mathrm{d}u=-\int_0^{u(t)} m\cdot\ddot{u}_{\mathrm{g}}(t)\,\mathrm{d}u \tag{2}$$

Introducing $\mathrm{d}u=\dot{u}\mathrm{d}t$ and integrating over the entire duration of an earthquake (t), the relative energy equation can be rearranged as shown in Eq. (3):

$$\frac{m\cdot\dot{u}^2}{2}+\int_0^t c\cdot\dot{u}^2\mathrm{d}t+\int_0^t f_{\mathrm{s}}(u)\cdot\dot{u}\,\mathrm{d}t=-\int_0^t m\cdot\ddot{u}_{\mathrm{g}}(t)\cdot\dot{u}\,\mathrm{d}t \tag{3}$$

Equation (3) may be stated in general type of energy components as below:

$$E_{\mathrm{K}}+E_{\xi}+E_{\mathrm{S}}=E_{\mathrm{I}} \tag{4}$$

where E_K represents the relative kinetic energy, E_{ξ} stands

for the damping energy and E_S is the total absorbed energy. The energy component on the right-hand side of Eq. (4) indicates the relative earthquake input energy (E_I), or in other words, the energy demand. Meanwhile, the total energy dissipated by the structure is composed of two parts as elastic strain energy (E_{Se}), and hysteretic energy (E_p) which is the main energy component in nonlinear behavior, i.e. the plastic strain energy. So that Eq. (4) can be written as:

$$E_K + E_\xi + \left[E_{Se} + E_p \right] = E_I \tag{5}$$

Since the summation of E_K and E_{Se} constitutes the total elastic energy (E_e) of SDOF system, Eq. (5) can be rearranged as:

$$E_e + E_\xi + E_p = E_I \tag{6}$$

The energy balance equation may also be expressed as follows by taking the energy component dissipated by the inherent damping (E_ξ) to the right-hand side of Eq. (6):

$$E_e + E_p = E_I - E_\xi = E_D \tag{7}$$

Since the part of seismic input energy will be dissipated by E_ξ as earthquake induced ground motion ends, the difference between E_I and E_ξ appearing in Eq. (7) indicates the energy input that contributes to damage of structures (E_D), and originally denominated by Housner (1956). Once E_I is computed via the design input energy spectra, the energy conducing to structural damage to a great extent can be predicted as the multiplication of input energy (E_I) with a factor λ, which depends on the damping ratio (ξ), ductility (μ) and the cumulative ductility factor (η). Introducing λ, the modification factor of earthquake energy input, in Eq. (7), yields the energy balance equation given by Eq. (8):

$$E_e + E_p = \lambda \cdot E_I \tag{8}$$

Although there are many empirical studies (Akiyama, 1985; Kuwamura and Galambos, 1989; Fajfar and Vidic, 1994; Benavent-Climent *et al*., 2002; Benavent-Climent *et al*., 2010) about the estimation of λ factor, in this study the modification factor defined as a function of a structural damping by Akiyama (1985) is used:

$$\lambda = \left(1 + 3 \cdot \xi + 1.2 \cdot \sqrt{\xi}\right)^{-2} \tag{9}$$

Modelling of component hysteretic behavior, which have direct influence on energy dissipation capacity, is essential for the accurate estimation of energy-based base shears. The energy dissipation capacity of RC members subjected to reverse cyclic loading decreases due to combined effects of degradation of stiffness and strength and pinching effects, which are particularly common in RC members. The area surrounded by loops of the hysteretic model with moderate or severe pinching behavior is smaller than the area of the hysteresis loops of elasto-plastic or strength hardening non-degrading piecewise linear hysteretic models, which have stable hysteresis loops. Also, if a structural member exhibits some level of stiffness degradation or experiences a strength degradation due to increasing inelastic displacements or repeated cyclic load reversals, the area enclosed by the hysteresis loops will decrease. Therefore; the reduced hysteretic model of RC structural members should be considered while the dissipated energy is computed and the hysteretic (or plastic) energy of the system for the stable models (generally elasto-plastic or bilinear strength hysteretic model) should be modified with a factor (η_p) to consider the reduced hysteresis rules (Bai and Ou, 2012). Accordingly, the modified energy balance equation, which is acceptable for all structural systems, can be written as:

$$E_e + \eta_p \cdot E_p = \lambda \cdot E_I \tag{10}$$

Utilizing of the plastic energy modification factor (η_p) provides a practical approach in structural design to account for the reduction in the area of hysteresis loops of RC members, which are not stable and smooth. Otherwise, calculation of irrecoverable hysteretic energy based on stable hysteresis loops will overestimate the energy dissipation capacity resulting in excessive damage. Figure 1 shows the smooth and the reduced hysteresis loops together, where A_F stands for the area of full hysteresis loop, and A_P represents the area of hysteresis loop with strength degradation and pinching effects. Δ_y is the yielding displacement, Δ_{max} is the maximum displacement and K_i and K_{eff} are the elastic and the effective stiffnesses, respectively. The r indicates the post-yield stiffness or the second-slope stiffness ratio and rK_i is the slope (secondary stiffness) of the hysteresis loop. R-P-P is the rigid-perfectly-plastic hysteresis loop as mentioned in Jacobsen's approach to obtain the equivalent damping value (Jacobsen, 1930; Dwairi, 2004).

Accordingly, the modification factor of plastic energy (η_p) is given by:

$$\eta_p = \frac{A_p}{A_F} = \frac{A_{RPP}}{A_F} \cdot \frac{A_p}{A_{RPP}} = \left[\frac{\mu \cdot (1 + r \cdot \mu - r)}{(\mu - 1) \cdot (1 - r)} \right] \cdot \frac{A_p}{A_{RPP}} \tag{11}$$

where $\mu = \Delta_{max}/\Delta_y$ is the displacement ductility demand of the structural member. In Eq. (11), the ratio of A_{RPP}/A_F can easily be obtained in terms of μ and r by using the rectangular area of R-P-P model and the trapezoid area of bilinear model (Fig. 1).

The ratio of A_p/A_{RPP} is derived using the concept of modelling of the hysteretic damping with the equivalent viscous damping concept (Blandon and Priestley, 2005; Rodrigues *et al*., 2012). The equivalent viscous damping (ξ_{eq}) is often expressed as the summation of the initial

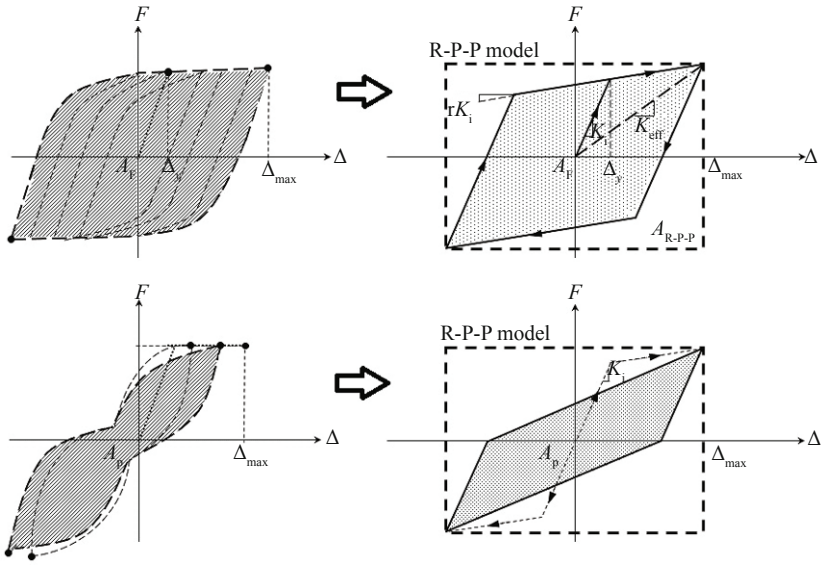

Fig. 1 Smooth and reduced (pinched) hysteresis models

elastic damping (ξ_0) and the hysteretic damping (ξ_H):

$$\xi_{eq} = \xi_0 + \xi_H \tag{12}$$

The elastic damping component (ξ_0) is commonly accepted as 5% for typical RC structures. However, the hysteretic damping representing the dissipation of energy due to nonlinear behavior depends essentially on the inelastic characteristics of structural members. Jacobsen (1930) defined the hysteretic damping ratio by using the energy dissipated in harmonic vibration. By integrating the second energy component on the left-hand side of Eq. (3) from $t = 0$ to $t = 2\pi/\omega$, the energy dissipated by viscous damping per cycle (E_ξ) is obtained as (Chopra, 1995):

$$E_\xi = \pi \cdot c \cdot \omega \cdot u_0^2 = 2 \cdot \pi \cdot \xi \cdot \frac{\omega}{\omega_n} \cdot k \cdot u_0^2 \tag{13}$$

where ω is the frequency of harmonic loading, ω_n is the natural circular frequency, k is the stiffness and u_0 is the displacement amplitude. As illustrated in Fig. 2, the dissipated energy (E_{dis}) is equal to the area inside the hysteresis loop and E_{sto} stands for the elastic strain energy stored by the system. With reference to Fig. 2, the hysteretic damping may be approximated by equating the energy dissipated in viscous damping to the energy dissipated in the inelastic behavior (the area of hysteresis loop). Finally, assuming that the frequency of the excitation is equal to the natural frequency of free vibration ($\omega = \omega_n$), the equation of hysteretic damping is determined as:

$$\xi_H = \frac{1}{4\pi} \cdot \frac{E_{dis}}{E_{sto}} \tag{14}$$

It is quite evident that the structural response to earthquake induced ground motions cannot be exactly represented by steady-state vibration and accordingly,

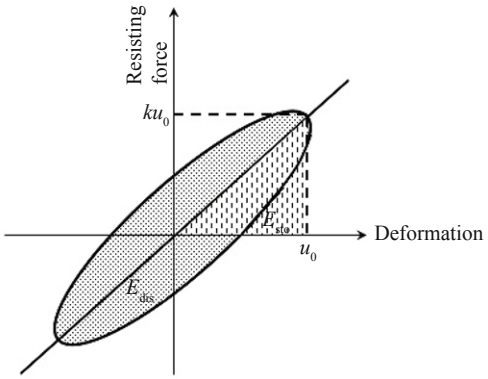

Fig. 2 Dissipated energy in a cycle of harmonic vibration and elastic strain energy

the shape of hysteresis loop will not be exactly an ellipse. Consequently, there are some empirical proposals in literature regarding the equivalent damping in RC members subjected to uniaxial loadings (Priestley *et al*., 2007; Dwairi *et al*., 2007). If combined stiffness and strength degradation, and pinching effects are considered, the simplest approach proposed by Jacobsen to estimate the hysteretic damping as a function of A_p/A_{RPP} can be used (Khan *et al*., 2016):

$$\xi_H = \frac{2}{\pi} \cdot \frac{A_p}{A_{RPP}} \tag{15}$$

For the theoretical R-P-P hysteresis loop dissipating more energy in comparison to available hysteretic models, the hysteretic damping value is found to be $2/\pi$ by using Jacobsen›s approximation.

Utilizing A_p/A_{RPP} ratio of Eq. (15) in Eq. (11), leads to the following equation of plastic energy modification factor (η_p):

$$\eta_{\mathrm{p}}=\frac{\pi\cdot\mu\cdot(1+r\cdot\mu-r)}{2\cdot(\mu-1)\cdot(1-r)}\cdot\xi_{\mathrm{H}} \tag{16}$$

Many approaches and formulas are available in the scientific literature for estimation of hysteretic damping (ξ_{H}) considering different hysteretic models (Gulkan and Sozen, 1974; Kowalsky, 1994; Priestley, 2003; Blandon and Priestley, 2005; Dwairi *et al*., 2007). Among them, the latest one proposed by Dwairi *et al*. (2007) is used in this study, which accounts for the effect of hysteretic behavior and can easily be implemented in simplified design methods:

$$\xi_{\mathrm{H}}=C_{\mathrm{LT}}\cdot\left(\frac{\mu-1}{\pi\cdot\mu}\right)\% \tag{17}$$

In Eq. (17), constant C_{LT} depends on hysteresis rule and effective period (T_{eff}). For large Takeda hysteretic model, which is suitable for RC frame type structures, if $T_{\mathrm{eff}}<1\,\mathrm{s}$ then $C_{\mathrm{LT}}=65+50\cdot(1-T_{\mathrm{eff}})$ and, if $T_{\mathrm{eff}}\geq1\,\mathrm{s}$ then $C_{\mathrm{LT}}=65$.

3 Elastic vibrational energy

Elastic vibrational energy comprises the relative kinetic energy as well as the elastic strain energy and this component of energy is related with the linear-elastic part of Fig. 3, where the graphical interpretation of elastic and plastic energies together with the modification factors η_{p} and λ is shown. Akiyama (1985) revealed that the elastic vibrational energy may be determined with a judicious accuracy by presuming MDOF system to be reduced into an equivalent SDOF system. Accordingly, the elastic energy may be estimated with:

$$E_{\mathrm{e}}=\frac{1}{2}\cdot V_{\mathrm{y}}\cdot\Delta_{\mathrm{y}}=\frac{1}{2}\cdot M\cdot\left[\frac{T_{\mathrm{e}}}{2\pi}\cdot\frac{V_{\mathrm{y}}}{W}\cdot\mathrm{g}\right]^2 \tag{18}$$

where V_{y} is the yield base shear force, Δ_{y} is the yielding displacement, W is the total seismic mass, T_{e} is the elastic vibrational period and g is the gravitational acceleration.

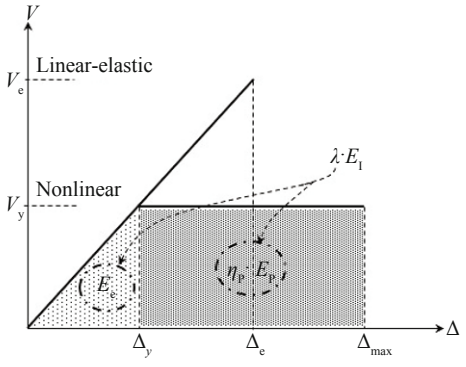

Fig. 3 Modified energy balance concept

4 Seismic input energy to MDOF system

It was shown by Housner (1956) that the pseudo velocity spectra of many major earthquakes tend to be almost constant over wide period ranges (Leelataviwat *et al*., 2002). According to this assumption, the seismic energy input to an equivalent *n*th mode SDOF system ($E_{I(SDOF)n}$) considering the elastic velocity response spectra ($S_{V,n}$) can be approximated as:

$$E_{I(SDOF)n}=\frac{1}{2}\cdot M_n\cdot S_{V,n}^2=\frac{1}{8}\cdot\frac{M_n\cdot T_n^2}{\pi^2}\cdot S_{a,n}^2 \tag{19}$$

where $M_n=\phi_n^T\cdot m\cdot\phi_n$ is the generalized mass, ϕ_n is the natural mode vector of the *n*th mode and *m* is the mass matrix. Equation (19) can also be written using pseudo-acceleration ($S_{a,n}$,) and the natural period (T_n) of the *n*th mode.

Since it enables a clear understanding of derivation of seismic energy input to MDOF system, the governing equation of motion of a nonlinear MDOF system is formulated in terms of modal coordinates $q_n(t)$ as (Chopra, 1995):

$$\ddot{q}_n(t)+2\cdot\xi_n\cdot\omega_n\cdot\dot{q}_n(t)+\frac{f_n}{M_n}=-\Gamma_n\cdot\ddot{u}_{\mathrm{g}}(t) \tag{20}$$

where ξ_n represents the damping ratio and ω_n is the natural circular frequency of *n*th mode of vibration, respectively, f_n is the nonlinear restoring force vector, and Γ_n is the modal participation factor of the *n*th vibration mode and is determined as indicated above:

$$\Gamma_n=\frac{\phi_n^T\cdot m\cdot 1}{\phi_n^T\cdot m\cdot\phi_n} \tag{21}$$

where 1 is a *N*th order influence vector with each element equal to unity.

When compared to the governing equation of motion of nonlinear SDOF system (Eq. (1)), it is clear that magnifying the earthquake excitation by Γ_n results in the magnification of seismic input energy by Γ_n^2. Accordingly, once relative earthquake input energy of each equivalent SDOF system (i.e., SDOF system with free vibration characteristics of the *n*th mode of MDOF system) is estimated we only need to perform modal analysis to get Γ_n and then $E_{I(SDOF)n}$ is converted to the relative input energy contribution of *n*th mode of MDOF system ($E_{I(MDOF)n}$) as:

$$E_{I(MDOF)n}=E_{I(SDOF)n}\cdot\Gamma_n^2 \tag{22}$$

The term "relative" is related to the definition of input energy since integrating the governing equation of motion of SDOF system in time domain on relative displacement with respect to ground leads to relative energy equation. The relative earthquake input energy

of MDOF system may be estimated considering the superposition of energies related to the first few vibration modes (Kalkan and Kunnath, 2007). Therefore, the total earthquake energy input to MDOF system is approximated by means of modal energy-decomposition approach as indicated below:

$$E_{I(MDOF)} = \sum_{n=1}^{N=3} E_{I(SDOF)n} \cdot \Gamma_n^2 = E_{I(SDOF)1} \cdot \Gamma_1^2 + E_{I(SDOF)2} \cdot \Gamma_2^2 + E_{I(SDOF)3} \cdot \Gamma_3^2 \quad (23)$$

5 Derivation of energy-based ultimate base shear force including P-delta effects

The derivation of energy-based ultimate base shear force including P-delta effects is directly based on a certain pre-selected failure mechanism and involves considerable inelastic (plastic) state of a structure. Although frame structures may experience different failure mechanisms, the global failure mechanism, where flexural plastic deformations concentrate first at the end of beam elements and then at the bottom end of the first story columns, is always preferable in seismic design since this type of mechanism leads to a ductile collapse by satisfying strong column-weak beam design principle (Fig. 4). Additionally, global failure mechanism may increase the energy dissipation capacity by imposing less ductility demand on structural members through other possible failure modes, and exhibits a more uniform interstory drift pattern (Bai and Ou, 2015). In local or soft-story failure mechanisms plastic hinges occur at both ends of particular story columns and hence the stability of vertical members under gravity loads may not be preserved causing a catastrophic collapse. So, these types of mechanisms are not considered in seismic design.

P-delta effects are usually negligible in elastic design methodology, which is performed by assuming that at design loads structures behave in a linearly elastic manner. But, when the structure is considered at its ultimate state, the destabilising influence of gravitational loads, i.e. the P-delta effects, may become significant due to large inelastic lateral deformations. Furthermore, as number of story increases, P-delta effects become more important. It is possible to account for P-delta effects in order to derive energy-based ultimate base shear force.

Considering the pre-selected failure mechanism of Fig. 4, the moment of external forces about the baseline can be written as:

$$M = \sum_{i=1}^{N} F_i \cdot H_i + \Delta F_N \cdot H_N + \sum_{i=1}^{N} w_i \cdot H_i \cdot \theta_u \quad (24)$$

where F_i is the lateral load at story level i, ΔF_N is the portion of the base shear force assumed to be concentrated at top level N in addition to F_N, H_i and H_N is the height of levels i and N, respectively. w_i is the gravitational load acting at story level i and θ_u is drift ratio targeted in the design and also supposed to be almost constant throughout the structure height for simplicity.

Rearranging Eq. (24) leads to:

$$M = \sum_{i=1}^{N} H_i \cdot \left(F_i + w_i \cdot \theta_u\right) + \Delta F_N \cdot H_N = \sum_{i=1}^{N} H_i \cdot \left(F_i + \Delta F_i^{P-\Delta}\right) + \Delta F_N \cdot H_N \quad (25)$$

where $\Delta F_i^{P-\Delta} = w_i \cdot \theta_u$ represents the additional lateral force acting at each floor level due to P-delta effect.

One can easily recognize from Eq. (25), the lateral design seismic force applied to level i including P-delta effect ($F_i^{P-\Delta}$) is:

$$F_i^{P-\Delta} = F_i + \Delta F_i^{P-\Delta} = \alpha_i \cdot \left(V_y - \Delta F_N\right) + w_i \cdot \theta_u \quad (26)$$

where $\alpha_1+\alpha_2+\ldots+\alpha_N = 1$. It is obvious that smaller lateral forces (F_i) are required when P-delta effects are considered.

Accordingly, the external work done by both the equivalent inertial and gravitational forces is equal to:

$$E_{\mathrm{p}} = \left(\sum_{i}^{N} F_i^{P-\Delta} + \Delta F_N\right) \cdot \Delta_{\mathrm{p}} = \sum_{i}^{N} F_i^{P-\Delta} \cdot H_i \cdot \theta_{\mathrm{p}} + \Delta F_N \cdot H_N \cdot \theta_{\mathrm{p}} \quad (27)$$

where θ_{p} is the plastic base rotation.

Considering an inverted triangular lateral force distribution, the inertial force acting on each floor level can be associated with the base shear (V_{y}) by Eq. (28) as:

$$F_i = \frac{w_i \cdot H_i}{\sum_{j=1}^{N} w_j \cdot H_j} \cdot \left(V_{\mathrm{y}} - \Delta F_N\right) = \alpha_i \cdot \left(V_{\mathrm{y}} - \Delta F_N\right) \quad (28)$$

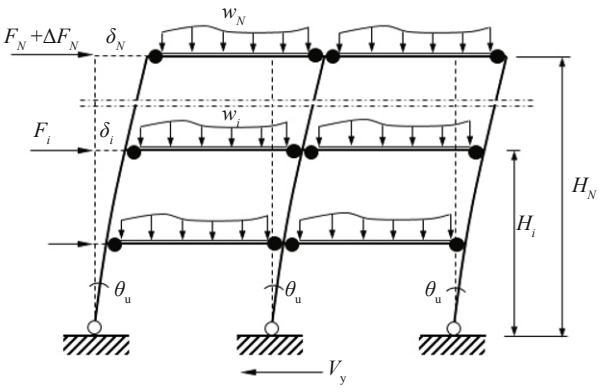

Fig. 4 Pre-selected failure mechanism

The additional lateral seismic force acting on the top, ΔF_N, can also be related to base shear in accordance with TSDC (2007):

$$\Delta F_N = 0.0075 \cdot N \cdot V_y \tag{29}$$

where N is the story number.

Substituting $F_i^{P-\Delta}$ from Eq. (26) and ΔF_N from Eq. (29) to Eq. (27) leads:

$$E_p = \left(\sum_{i=1}^{N} \alpha_i \cdot H_i \cdot (1 - 0.0075 \cdot N) + 0.0075 \cdot N \cdot H_N \right) \cdot \theta_p \cdot V_y + \left(\sum_{i=1}^{N} w_i \cdot H_i \right) \cdot \theta_p \cdot \theta_u \tag{30}$$

The second term on the right-hand side of Eq. (30) represents the work done by gravitational forces. This term can be treated as geometric energy term (E_G), which is originally introduced by Hernández-Montes *et al*. (2015) to account for P-delta effects on dynamic response of nonlinear SDOF systems. The geometric energy term can be included in the equation of motion in terms of energy and can be shown as external load acting along with E_I.

The energy-based ultimate base shear force is derived from classical work-energy principle equating the modified plastic energy of MDOF systems to the external work done by the equivalent inertial forces and the gravitational forces. First, the plastic energy equation is expressed in terms of η_p and λ modification factors by rearranging Eq. (10). Elastic vibrational energy (E_e) from Eq. (18) and MDOF nth mode input energy contribution ($E_{I(MDOF)n}$) from Eq. (22) are substituted in Eq. (10) and then is equated to Eq. (30). Finally, following the necessary arrangements, a quadratic equation in terms of V_y is obtained as below:

$$\left(\frac{T_e^2}{8\pi^2} \cdot \frac{g}{W} \right) V_y^2 + \eta_p \cdot \theta_p \cdot \left(\sum_{i=1}^{N} \alpha_i \cdot H_i \cdot (1 - 0.0075 \cdot N) + 0.0075 \cdot N \cdot H_N \right) V_y + \eta_p \cdot \sum_{i}^{N} w_i \cdot H_i \cdot \theta_p \cdot \theta_u - \lambda \cdot \sum_{i=1}^{N} \Gamma_n^2 \cdot E_{I(SDOF)n} = 0 \tag{31}$$

Once η_p and λ modification factors are estimated and θ_u is considered at the beginning, energy-based ultimate base shear force accounting for P-delta effects can be readily obtained by solving Eq. (31). While P-delta effect is not included, the term of Eq. (31) incorporating gravity loads (w_i) will drop automatically. Finally, dividing energy-based base shear force to seismic weight yields energy-based base shear force coefficient (V_y/W).

The base shear force is completely obtained from energy balance equation, so the all energy terms should be included explicitly in the equation. Accordingly, it seems reasonable to implement nonlinear dynamic analysis in order to obtain each energy response parameter. However, using nonlinear dynamic analysis would be unpractical for design purposes. So, simple yet realistic base shear formula considering the energy balance of the structure in inelastic range is derived. Accordingly, the authors show tendency to use the commonly accepted approximate methods relating to the estimation of energy components. Consequently, these approximations may lead to different base shear forces. Computing the energy components by means of nonlinear time history analysis and relating them to base shear force to be used in design may provide an opportunity to compare the resultant base shear forces of the study.

6 Case study

Theoretical RC frame structures having regular masses and rigidities are used in order to determine the energy-based base shear force coefficients including P-delta effects. All of the considered structures are typical RC frames consisting of beams and columns without shear walls.

6.1 Description and design of RC frames

The 3 to 8 story 3 bay moment resisting frames are seismically designed and properly detailed according to the requirements of TSDC (2007) considering both gravity and seismic loads and as well as TS500 (2000). The characteristic compression strength of concrete is taken to be 20 MPa, and the characteristic yield strength of both longitudinal and transverse reinforcement steel is 420 MPa. Frames are assumed to be in seismic zone 1 and the site condition is chosen as Z3 according to TSDC (2007). In TSDC (2007), the design base shear force is calculated considering the 5% damped elastic design spectrum and it is reduced depending on the structural characteristics of the system by the response reduction factor (R_a). The elastic spectrum coefficient ($S(T_1)$) is determined as a function of natural period (T_1) and corner periods (T_A and T_B) depending on soil conditions. The spectral acceleration coefficient ($A(T_1)$) is given as a product of the seismic zone coefficient (A_0), the building importance factor (I) and $S(T_1)$. Accordingly, the design base shear coefficient is calculated as $V/W = A(T_1)/R_a(T_1)$. Rectangular beams and square columns are considered in RC design and the design of frames is performed using the structural analysis program SAP2000 (2016).

Figure 5 describes the geometry of 3 to 8 story frames used in the analyses. The story heights (H_i), span lengths of frame model, uniformly distributed dead (g_i) and live (q_i) loads in all spans and concentrated dead and live loads acting on exterior and interior beam-column joints denoted as (G_{ei}, Q_{ei}) and (G_{ii}, Q_{ii}) are shown on this figure as well.

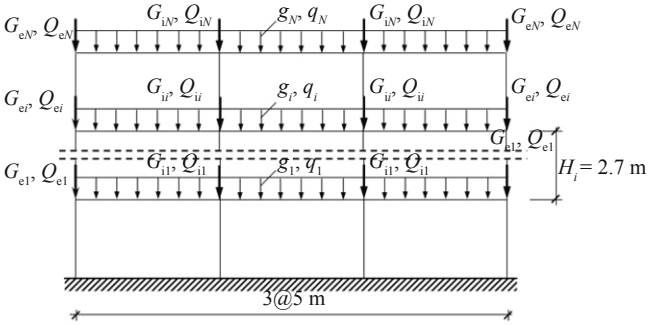

Fig. 5 Frame model and gravity loads

Table 1 lists the magnitude of distributed and concentrated gravity loads. The selected frame is 2D modeling of an internal frame of a 3D structure which has symmetrical distribution of stiffness in all directions and uniform mass distribution on the plan and the magnitudes of gravity loads are determined accordingly. Live load participation factor (n) is taken as 0.30 and floor weights and related masses, which are considered in seismic calculations, are determined as the combination of dead loads and 30% of live loads.

6.2 Energy-based base shear force coefficients and comparison with pushover results

Seismic input energy of an equivalent nth mode SDOF system, thereby of MDOF system, is a function of natural periods and modal vectors. Additionally, calculation of plastic energy modification factor (η_p) makes essential the estimation of the ductility ratio (μ), which can be calculated from pushover analysis. Thereby, two-dimensional nonlinear mathematical model of each frame is created in SAP2000. Initial effective stiffness values of RC components are reduced according to TSDC (2007) on account of cracking during the inelastic response of frames. Beams and columns are modeled as nonlinear structural components with lumped plasticity by assigning plastic hinges at both ends. Force-displacement capacity boundaries (i.e., backbone curves) of the components are defined in accordance with FEMA-356 (2000).

Some fundamental dynamic parameters determined from eigenvalue analysis of frames, the seismic input energy of the equivalent nth mode SDOF system and seismic input energy of MDOF system are listed in Table 2, where T_n is the natural period of the nth mode, $L_n = \phi_n^{\mathrm{T}} \cdot m \cdot 1$, α_n is the effective modal mass participating ratio of the nth mode and $m_{\mathrm{eff}n}$ is the effective modal mass of the nth mode, respectively.

The seismic input energy of the equivalent nth mode SDOF system is approximated using the design acceleration spectrum of TSDC (2007). The post-yield stiffness (r) is assumed as 10% of the initial elastic stiffness. Damping ratio (ξ) is taken to be 5% and the corresponding value of seismic input energy modification factor (λ) is calculated from Eq. (9). For the probability level of exceedance 10% in 50-year period (the design earthquake level), the maximum interstory drift ratio (θ_u) is suggested as 2% (Bayat *et al*., 2008; Liao, 2010). The design earthquake of TSDC (2007) corresponds to this probability and $\theta_u = 0.02$ is considered accordingly. The return period of the design earthquake is 475 years (the probability of exceedance in 50 years is 10%) for buildings having importance factor of 1 and 2475 years (the probability of exceedance in 50 years is 2%) for buildings having importance factor of 1.5. Finally, the plastic base rotation is calculated as θ_u-θ_y, where θ_y is determined individually for each frame from pushover analysis.

The energy-based base shear force coefficients including and not including the effect of P-delta are compared to the results of pushover analysis. Since all the frames satisfy strong column–weak beam principle of design and the derivation of energy-based base shear force coefficients is mainly focused on this failure mechanism, this comparison can be reasonably acceptable. In pushover analysis, beams and columns are modeled as nonlinear structural members by assigning plastic sections at the end parts of these members and an invariant lateral load distribution which corresponds to the first-mode shape is used. Frames are pushed up to $\delta/H_N = 0.02$, which is also considered in determination of energy-based base shear force coefficients. Pushover curves excluding and including the influence of P-delta effects are illustrated in Fig. 6. The vertical axis of pushover curve is base shear force coefficient (V/W) and the horizontal axis is roof drift ratio (δ/H_N).

Energy-based base shear force coefficients obtained using the derived equation in the study, pushover-based base shear force coefficients corresponding to 2% drift ratio and code-based ones are summarized in Table 3. Energy-based base shear force coefficients reflect the expected decreasing trend in strength (and therefore stiffness) while P-delta effects are implemented in the analysis. Meanwhile, base shear force capacity of the system reduces due to consideration of P-delta effects in

Table 1 Magnitude of gravity loads

Uniform loads (kN/m)							
g_i		q_i		g_N		q_N	
20.50		6.67		15.50		5.00	
Concentrated loads (kN)							
G_{ei}	Q_{ei}	G_{ii}	Q_{ii}	G_{eN}	Q_{eN}	G_{iN}	Q_{iN}
71.00	16.65	102.63	33.33	52.50	12.50	77.45	25.00

Table 2 Equivalent SDOF system properties of frames and seismic input energy of MDOF system

Frame		T_n (s)	L_n (tons)	M_n (tons)	α_n (%)	$m_{eff,n}$ (tons)	Γ_n	$E_{I(ESDOF)n}$ (kNm)	$E_{I(MDOF)n}$ (kNm)	$E_{I(MDOF)}$ (kNm)
3-story	1	0.607	142.508	110.736	86.71	183.401	1.287	48.838	80.894	81.902
	2	0.188	-57.239	147.459	10.50	22.209	-0.388	6.352	0.956	
	3	0.104	58.296	575.968	2.79	5.901	0.101	5.056	0.052	
4-story	1	0.746	187.597	143.954	83.47	244.458	1.303	68.898	116.976	119.185
	2	0.228	-71.569	158.233	11.05	32.362	-0.452	10.026	2.048	
	3	0.120	58.461	289.853	4.03	11.803	0.202	3.940	0.161	
5-story	1	0.884	234.520	178.973	81.47	307.294	1.310	91.590	157.178	161.220
	2	0.269	-86.369	178.796	11.06	41.717	-0.483	15.769	3.679	
	3	0.139	64.807	249.324	4.47	16.860	0.260	5.366	0.363	
6-story	1	1.024	283.344	215.576	80.11	372.412	1.314	117.123	202.224	208.914
	2	0.311	-102.157	204.333	10.99	51.090	-0.500	24.088	6.022	
	3	0.160	72.512	245.969	4.60	21.384	0.295	7.675	0.668	
7-story	1	1.206	331.710	253.126	79.60	434.665	1.310	146.815	251.949	262.919
	2	0.372	-117.071	234.916	10.70	58.429	-0.498	39.623	9.827	
	3	0.196	78.890	254.081	4.49	24.519	0.310	11.897	1.143	
8-story	1	1.341	383.260	291.808	78.76	503.369	1.313	176.960	305.074	320.834
	2	0.412	-134.244	264.387	10.66	68.130	-0.508	54.699	14.116	
	3	0.216	88.727	271.993	4.53	28.952	0.326	15.467	1.644	

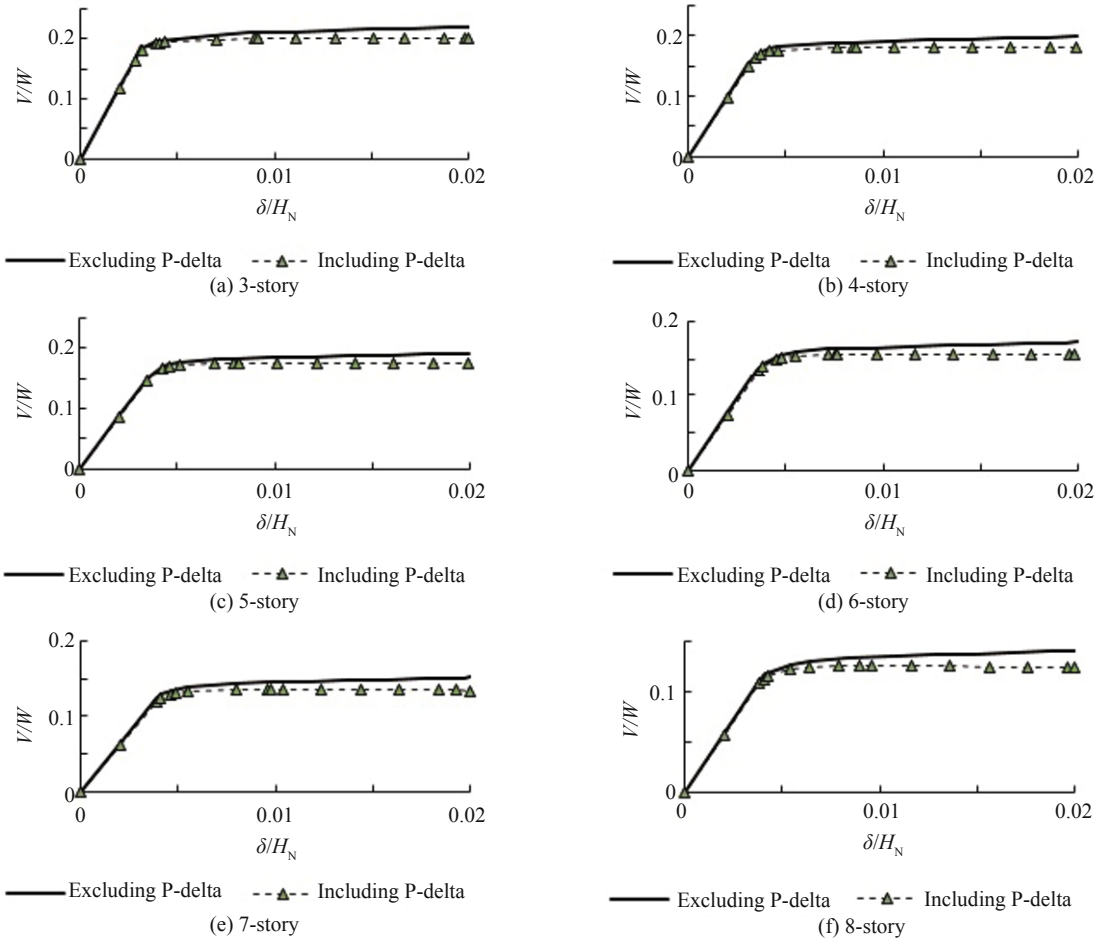

Fig. 6 Pushover curves of frames

energy-based analysis. As number of stories increases, energy-based base shear force coefficients excluding or including P-delta effects decrease. These are verified by means of pushover analysis. Also when the number of stories increases, P-delta effects become more important (e.g., in 3-story frame the decrease in V_y/W when P-delta effect is considered is 5.8%, while it is 6.1% in 7-story frame). However, the variation is limited since the resultant P-delta effects are properly controlled by the adequate lateral stiffness of the frame models. This variation is more obvious in pushover-based base shear force coefficients when compared to energy-based ones. Energy-based base shear coefficients vary between 1.8 and 2.1 times of design base shear coefficients, while the ratio of pushover-based coefficients to code-based ones is between 1.35 and 1.60. While considering P-delta effects in analyses, the ratio of energy-based base shear coefficients to code-based ones decreases (the variation is between 1.70 and 1.95).

Frame models behave almost elastically until 0.4% roof drift level. The slope of the initial stiffness curve is slightly decreased in its elastic part of lateral deformation. The post-yield stiffness ratio of the frame reduces due to P-delta effects and starts to generate a negative post-yield stiffness.

6.3 NLTH analysis of structural models

A total of ten real accelerograms are selected regarding to the magnitude, distance, fault type, and soil profile type information. The accelerograms with a magnitude range of $6.5 \le M_w \le 7.5$ and source-to-site distances (R_{JB}) less than 50 km are compiled from PEER-NGA strong ground motion database, which is used as the main source (PEER, 2016). Since all frames are assumed to be in Z3-type site class, the site conditions of the accelerograms represent the features of Z3 soil. Soil profile type definitions of Z3 is considered as the counterpart of NEHRP D site class, which is classified as $180 \le V_{S30} \le 360$. The selected ground motions have strike-slip fault mechanism and near-fault effects are not considered. The list of available ground motion records and the overall characteristics of accelerograms are presented in Table 4, where M_w is the moment magnitude of earthquake, R_{JB} is the Joyner-Boore distance, V_{S30} is the average shear-wave velocity to 30 m depth of subsoil, *PGA* is peak ground acceleration, *PGV* is peak ground velocity and *PGD* is peak ground displacement.

The selected real accelerograms are scaled in terms of amplitude in time domain to make them proper for the code-based seismic hazard level, which is traditionally defined in the form of 5% damped elastic response spectra of acceleration. The scaling procedure used herein is based on minimizing the differences between the scaled acceleration response spectrum and horizontal elastic design spectrum of TSDC for local site class Z3 by using the method of least-squares. This way, a total of ten scaled accelerograms fulfilling duration and

Table 3 Comparison of energy-based base shear force coefficients

Frame	Energy-based		Pushover		Design
	V_y/W	V_y/W (P-delta)	V_y/W	V_y/W (P-delta)	V/W (TSDC)
3-story	0.258	0.243	0.221	0.202	0.125
4-story	0.225	0.211	0.199	0.181	0.125
5-story	0.224	0.211	0.193	0.175	0.125
6-story	0.213	0.201	0.173	0.156	0.114
7-story	0.196	0.184	0.152	0.134	0.099
8-story	0.182	0.171	0.141	0.124	0.091

Table 4 Selected earthquake ground motions and major seismological parameters of records

Record name	Earthquake name	Recording station	M_w	R_{JB} (km)	V_{S30} (m/s)	*PGA* (g)	*PGV* (cm/s)	*PGD* (cm)
IMPVALL.I_I-ELC180	Imperial Valley-02, 1940	El Centro Array #9	6.95	6.09	213.44	0.281	30.93	8.66
IMPVALL.I_I-ELC270	Imperial Valley-02, 1940	El Centro Array #9	6.95	6.09	213.44	0.211	31.29	24.18
SUPER.B_B-POE360	Superstition Hills-02, 1987	Poe Road	6.54	11.16	316.64	0.286	29.02	11.56
BIGBEAR_HOS180	Big Bear-01, 1992	San Bernandino-E & Hospitality	6.46	34.98	296.97	0.101	11.85	3.36
KOBE_KAK000	Kobe, 1995	Kakogawa	6.9	22.5	312.0	0.240	20.80	6.39
KOBE_SHI000	Kobe, 1995	Shin-Osaka	6.9	19.4	256.0	0.225	31.33	8.38
KOCAELI_DZC180	Kocaeli, 1999	Duzce	7.51	13.6	281.86	0.312	58.85	44.05
DUZCE_DZC270	Duzce, 1999	Duzce	7.14	0	281.86	0.515	84.29	47.99
SIERRA.MEX_CHI090	El Mayor-Cucapah, 2010	Chihuahua	7.2	18.21	242.05	0.197	34.03	31.22
SIERRA.MEX_GEO090	El Mayor-Cucapah, 2010	Cerro Prieto Geothermal	7.2	8.88	242.05	0.288	49.54	40.31

Table 5 Some parameters of scaled accelerograms

Record name	Record duration (s)	Bracketed duration (s)	α_{ST}	$S_{ae}(T_0)$ (g)
IMPVALL.I_I-ELC180	53.710	30.160	1.58	0.4449
IMPVALL.I_I-ELC270	53.450	30.600	2.07	0.4360
SUPER.B_B-POE360	22.290	20.130	1.63	0.4653
BIGBEAR_HOS180	99.990	38.590	3.99	0.4021
KOBE_KAK000	40.950	25.710	2.02	0.4845
KOBE_SHI000	40.950	17.020	1.74	0.3912
KOCAELI_DZC180	27.180	19.920	1.41	0.4404
DUZCE_DZC270	25.880	19.020	0.87	0.4477
SIERRA.MEX_CHI090	129.995	76.070	2.01	0.3965
SIERRA.MEX_GEO090	99.995	53.515	1.35	0.3892

amplitude related requirements of TSDC for NLTH analysis are provided.

The scale factors (α_{ST}) providing the best match to elastic design spectrum of TSDC over a period range of interest (T_A = 0.01 s and T_B = 4.00 s) and some relevant parameters (duration, zero period spectral acceleration of scaled records ($S_{ae}(T_0)$)) that may be used to check the code requirements of accelerograms to be used in NLTH analysis are summarized in Table 5. Strong shaking duration is considered as bracketed duration defining as time interval length between the first and the last occurrence of an acceleration exceeding the certain threshold value of absolute 0.05 g. The mean of $S_{ae}(T_0)$ values of TSDC elastic design spectrum compatible ground motions is 0.43 g. The scaled accelerograms satisfy duration and amplitude related requirements of TSDC.

Figure 7 shows individual linear-elastic acceleration response spectra of scaled accelerograms, their median linear elastic response spectrum and the elastic design acceleration spectrum of TSDC for site class Z3, all developed for a damping ratio of 5%. Response spectra are constructed by using SeismoSpect software (SeismoSpect, 2016).

In order to compare the energy-based base shear force coefficients to those obtained from dynamic analysis, NLTH analyses of frames are performed by using the time histories of the scaled accelerograms complying with the elastic design acceleration spectrum of TSDC (2007). Direct integration method is used as the calculation method. Due to complexity of nonlinear

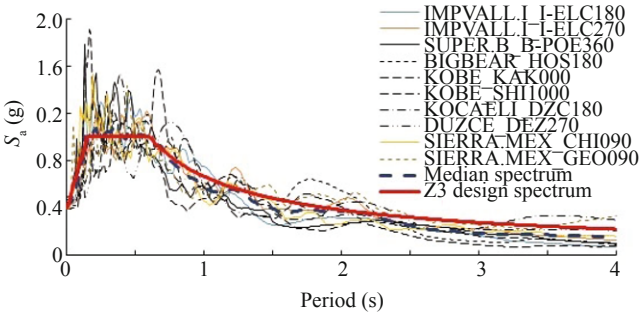

Fig. 7 Scaled spectra, median spectrum and design spectrum of TSDC

dynamic analysis of MDOF system, a relatively simple hysteretic model is preferred. Accordingly, a bilinear strength-hardening hysteretic model with post-yield stiffness ratio of 10%, which is compatible with the moment-rotation relationships of structural members, is used in SAP2000. Firstly, P-delta effects are not incorporated into nonlinear dynamic analyses. Since ten recorded accelerograms are selected, totally 60 NLTH analyses are performed considering the nonlinear structural models created in SAP2000 environment. Modal damping ratio is assumed as 5% and Rayleigh damping model, which assumes that the damping is proportional to a linear combination of stiffness and mass (Chopra, 1995), is used in dynamic analyses. Both the maximum base shear force coefficients and the average of the maximum values are summarized in Table 6.

The average base shear force coefficients of Table 6 indicate a very good correlation with the energy-based base shear force coefficients. It is found that energy-based base shear coefficients show better agreement with the average results of NLTH analyses rather than pushover-based base shear force coefficients (Fig. 8). The derived energy-balance equation considers the hysteretic behavior of RC members while monotonic force-deformation properties of members are implemented in pushover analysis. That this is the reason why energy-based base shear coefficients show better agreement with the average results of NLTH analyses rather than pushover-based base shear force coefficients. The last founding indicates the efficiency of the derived equation in the prediction of inelastic base shear capacity of frame structures.

Dynamic instability frequently occurs in NLTH analysis of frames while including P-delta effects in dynamic analyses. Accordingly, after the significant yielding systems undergo large lateral displacements, interstory drift ratios increase in one direction of the earthquake loading causing convergence problems and base shear forces cannot be obtained due to convergence problems. Large displacements cause enormous lateral force ($f_s(u)$) which leads to a sudden increase in the V/W coefficient. The variation of base shear force coefficient of 3- and 8-sory frames exposed to different earthquake ground motions are presented in Fig. 9 and Fig. 10,

Table 6 Base shear force coefficient results of NLTH

Record name	*V*/*W*					
	3-story	4-story	5-story	6-story	7-story	8-story
IMPVALL.I_I-ELC180	0.259	0.229	0.243	0.211	0.164	0.167
IMPVALL.I_I-ELC270	0.254	0.227	0.217	0.221	0.190	0.183
SUPER.B_B-POE360	0.253	0.239	0.236	0.205	0.186	0.178
BIGBEAR_HOS180	0.264	0.250	0.236	0.200	0.183	0.171
KOBE_KAK000	0.241	0.224	0.220	0.206	0.182	0.173
KOBE_SHI000	0.291	0.238	0.244	0.227	0.209	0.174
KOCAELI_DZC180	0.250	0.217	0.225	0.214	0.164	0.179
DUZCE_DZC270	0.258	0.236	0.216	0.202	0.170	0.163
SIERRA.MEX_CHI090	0.260	0.229	0.221	0.207	0.192	0.186
SIERRA.MEX_GEO090	0.247	0.221	0.229	0.199	0.180	0.176
Average	**0.258**	**0.231**	**0.229**	**0.209**	**0.182**	**0.175**

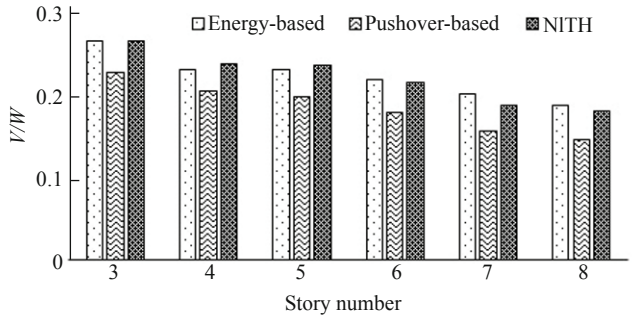

Fig. 8 Base shear force coefficients obtained from different analyses

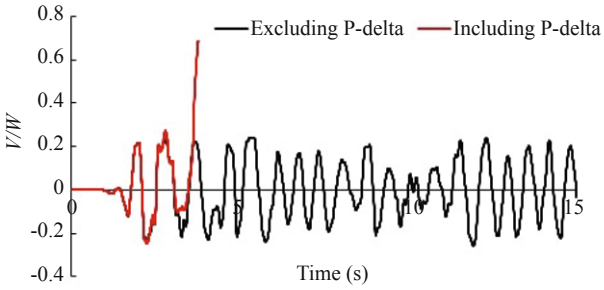

Fig. 9 Base shear force coefficient of 3-story frame due to IMPVALL.I_I-ELC180 ground motion

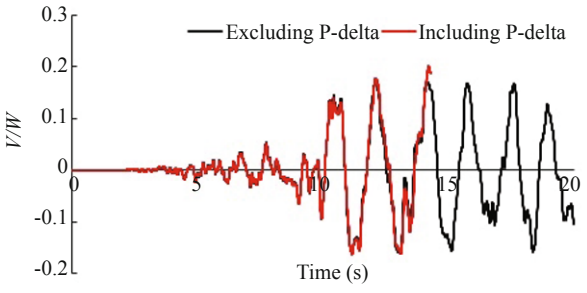

Fig. 10 Base shear force coefficient of 8-story frame due to BIGBEAR_HOS180 ground motion

respectively. Oscillation occurs while P-delta effects are not included in dynamic analyses. On the contrary, P-delta effects cause dynamic instability. Therefore, base shear forces including P-delta effects in NLTH analysis cannot imported.

7 Summary and conclusion

A modified energy-balance equation based on a pre-targeted failure mechanism and an ultimate target drift is derived considering the reduced hysteretic behavior of RC members and including P-delta effects. The modified plastic energy, which accounts for the reduction in the area of hysteresis loops of RC members and comprises seismic input energy modification factor, is equated to external work of both equivalent inertia forces and gravity loads. Relative seismic energy input to MDOF system is approximated by the sum of the energies related to the first three vibration modes and consequently the earthquake effect is considered as energy input to the structure. Pushover analysis and NLTH analysis using ten recorded accelerograms, which fulfill the duration and amplitude related requirements of TSDC, are performed and energy-based design base shear force coefficients are compared to the results of both nonlinear static analysis and nonlinear dynamic analysis.

Material nonlinearity, hysteretic properties of structural components and hysteretic damping are taken into account in a simple manner in the derived energy-based base shear force coefficients. The ductility and yield characteristics of the structure is explicitly considered in the derived equation. Moreover, P-delta effects are also included in the derived equations and the influence of P-delta action on energy-based base shear force coefficients is observed. While P-delta effects are incorporated into the analyses, energy-based base shear force coefficients decrease. Consequently, base shear force capacity of the system reduces when considering the influence of P-delta effects in energy-based analysis.

Energy-based base shear force coefficients excluding or including P-delta effects decrease, as number of stories increases. These results are also verified by means of pushover and NLTH analyses. A very good correlation between energy-based base shear force coefficients and the average base shear force coefficients of NLTH is observed. Energy-based base shear force coefficients are found to show better agreement with the average results of NLTH analyses rather than pushover-based base shear force coefficients. So it can be concluded that, the derived equation provides a reasonable confidence in estimation of the inelastic base shear force capacity of frame structures.

Since a global failure mechanism based on strong column–weak beam principle is considered as a failure mechanism, the obtained base shear force coefficients represent the nonlinear base shear force capacity of ductile frames. The derived equations provide a practical estimation of nonlinear base shear force capacity of frames without requiring time consuming inelastic modelling. It is evident that, estimation of nonlinear capacity of RC frames, which is essential in seismic design, requires considerable computational efforts and thus the derived equation, where the inelastic behavior of RC members is modeled by a plastic energy modification factor, can be used to define the capacity in a simple manner.

The base shear force obtained from the derived equation may be used in plastic design of structures, where the design of structures for a pre-selected failure mechanism is emphasized, in the context of performance-based seismic design. In the design process, using the base shear force obtained from the proposed formulation may reduce the local member damage since all of the energy is assumed to dissipate in the plastic hinges of the pre-selected failure mechanism. Moreover, it considers P-delta effects that may influence the capacity of members in plastic design.

In the proposed energy-based equation, the distribution of lateral forces along the stories is associated with the base shear force by assuming an inverted triangular distribution of lateral load which is generally valid when the first mode of vibration is dominant on the total dynamic response. Accordingly, the application of the proposed formulation is essentially limited to regular RC frame structures. However, the derived formulation can be extended to different types of structures by relating the total base shear force to different lateral force distributions including the higher mode effects.

References

Acun B and Sucuoğlu H (2010), "Performance of Reinforced Concrete Columns Designed for Flexure Under Severe Displacement Cycles," *ACI Structural Journal*, **107**(3): 364–371.

Adam C and Jager C (2011), "Seismic Induced Global Collapse of Non-deteriorating Frame Structures," in Papadrakakis M., Fragiadakis M., Lagaros, N.D., editors, *Computational Methods in Earthquake Engineering, Computational Methods in Applied Sciences*, **21**: 21–40.

Adam C and Jager C (2012), "Seismic Collapse Capacity of Basic Inelastic Structures Vulnerable to the P-Delta Effect," *Earthquake Engineering & Structural Dynamics,* **41**(4): 775–793.

Akbas B, Shen J and Hao H (2001), "Energy Approach in Performance-Based Seismic Design of Steel Moment Resisting Frames for Basic Safety Objective," *The Structural Design of Tall Buildings*, **10**(3): 193–217.

Akiyama H (1985), *Earthquake-Resistant Limit-State Design for Buildings*, The University of Tokyo Press, Japan.

Akiyama H (2002), "Collapse Modes of Structures Under Strong Motions of Earthquake," *Annals of Geophysics*, **45**(6): 791–798.

Alıcı FS and Sucuoğlu H (2016), "Prediction of Input Energy Spectrum: Attenuation Models and Velocity Spectrum Scaling," *Earthquake Engineering & Structural Dynamics*, **45**(13): 2137–2161.

Asimakopoulos AV, Karabalis DL and Beskos DE (2007), "Inclusion of P-Δ Effect in Displacement-Based Seismic Design of Steel Moment Resisting Frames," *Earthquake Engineering & Structural Dynamics*, **36**(14): 2171–2188.

Bai J and Ou J (2012), "Plastic Limit-State Design of Frame Structures Based on the Strong-Column Weak-Beam Failure Mechanism," *Proceedings of the 15th World Conference on Earthquake Engineering*, Lisboa, Portugal.

Bai J and Ou J (2015), "Realization of the Global Yield Mechanism of RC Frame Structures by Redesigning the Columns Using Column Tree Method", *Science China Technological Sciences*, **58**(10): 1627–1637.

Bayat MR, Goel SC and Chao SH (2008), "Further Refinement of Performance-Based Plastic Design of Structures for Earthquake Resistance," *14th World Conference on Earthquake Engineering*, Beijing, China.

Benavent-Climent A, Pujades LG and Lopez-Almansa F (2002), "Design Energy Input Spectra for Moderate Seismicity Regions," *Earthquake Engineering & Structural Dynamics*, **31**(5): 1151–1172.

Benavent-Climent A, Lopez-Almansa F and Bravo-Gonzales DA (2010), "Design Energy Input Spectra for Moderate-to-High Seismicity Regions Based on Colombian Earthquakes," *Soil Dynamics and Earthquake Engineering*, **30**(11): 1129–1148.

Blandon CA and Priestley MJN (2005), "Equivalent Viscous Damping Equations for Direct Displacement Based Design," *Journal of Earthquake Engineering*, **9**(2): 257–278.

Chao SH, Goel SC and Lee SS (2007), "A Seismic Design Lateral Force Distribution Based on Inelastic State of Structures," *Earthquake Spectra*, **23**(3): 547–569.

Choi H and Kim J (2006), "Energy-Based Seismic Design of Buckling-Restrained Braced Frames Using Hysteretic Energy Spectrum," *Engineering Structures*, **28**: 304–311.

Chopra AK (1995), *Dynamics of Structures, Theory and Applications to Earthquake Engineering*, Prentice Hall, Upper Saddle River, N.J.

Chou CC and Uang CM (2003), "A Procedure for Evaluating Seismic Energy Demand of Framed Structures," *Earthquake Engineering & Structural Dynamics*, **32**(2): 229–244.

Decanini LD and Mollaioli F (1998), "Formulation of Elastic Earthquake Input Energy Spectra," *Earthquake Engineering & Structural Dynamics*, **27**(12): 1503–1522.

Dindar AA, Yalçın C, Yüksel E, Özkaynak H and Büyüköztürk O (2015), "Development of Earthquake Energy Demand Spectra," *Earthquake Spectra*, **31**(3): 1667–1689.

Dwairi HM (2004), "Equivalent Damping in Support of Direct Displacement-Based Design with Applications to Multi-Span Bridges," *PhD Dissertation*, North Carolina State University, Raleigh, North Carolina.

Dwairi HM, Kowalsky MJ and Nau JM (2007), "Equivalent Damping in Support of Direct Displacement-Based Design," *Journal of Earthquake Engineering*, **11**(4): 512–530.

Fajfar P and Vidic T (1994), "Consistent Inelastic Design Spectra: Hysteretic and Input Energy," *Earthquake Engineering & Structural Dynamics*, **23**(5): 523–537.

FEMA-356 (2000), *Prestandard and Commentary for the Seismic Rehabilitation of Buildings*, Federal Emergency Management Agency, Washington, D.C.

Fenwick RC, Davidson BJ and Chung BT (1992), "P-Delta Actions in Seismic Resistant Structures," *Bulletin of the New Zealand National Society for Earthquake Engineering*, **25**(1): 56–69.

Gulkan P and Sozen MA (1974), "Inelastic Responses of Reinforced Concrete Structures to Earthquakes Motions," *ACI Journal Proceedings*, **71**(12): 604–610.

Hernández-Montes E, Aschheim MA and Gil-Martín LM (2015), "Energy Components in Nonlinear Dynamics Response of SDOF Systems," Nonlinear Dynamics, **82**(1): 933–945.

Housner GW (1956), "Limit Design of Structures to Resist Earthquakes," *Proceedings of the World Conference on Earthquake Engineering*, Berkeley, California.

Jacobsen LS (1930), "Steady Forced Vibrations as Influenced by Damping," *ASME Transactione*, **52**(1): 169–181.

Kalkan E and Kunnath SK (2007), "Effective Cyclic Energy as a Measure of Seismic Demand," *Journal of Earthquake Engineering*, **11**(5): 725–751.

Kalkan E and Kunnath SK (2008), "Relevance of Absolute and Relative Energy Content in Seismic Evaluation of Structures," *Advances in Structural Engineering*, **11**(1): 17–34.

Ke K, Chuan G and Ke S (2016), "Seismic Energy Factor of Self-Centering Systems Subjected to Near-Fault Earthquake Ground Motions," *Soil Dynamics and Earthquake Engineering*, **84**: 169–173.

Khan E, Kowlasky MJ and Nau JM (2016), "Equivalent Viscous Damping Model for Short-Period Reinforced Concrete Bridges," *Journal of Bridge Engineering*, **21**(2): 04015047.

Kim J, Choi H and Chung L (2004), "Energy-Based Seismic Design of Structures with Buckling-Restrained Braces," *Steel and Composite Structures*, **4**(6): 437–452.

Kowalsky MJ (1994), "Displacement Based Design: A Methodology for Seismic Design Applied to RC Bridge Columns," *MSc Dissertation*, University of California, San Diego.

Kuwamura H and Galambos T (1989), "Earthquake Load for Structural Reliability," *Journal of Structural Engineering*, **115**(6): 1446–1462.

Leelataviwat S, Goel SC and Stojadinovic B (2002), "Energy-Based Seismic Design of Structures Using Yield Mechanism and Target Drift," *Journal of Structural Engineering*, **128**(8): 1046–1054.

Leelataviwat S, Saewon W and Goel SC (2009), "Application of Energy Balance Concept in Seismic Evaluation of Structures," *Journal of Structural Engineering*, **135**(2): 113–121.

Liao WC (2010), "Performance-Based Plastic Design of Earthquake Resistant Reinforced Concrete Moment Frames," *PhD Dissertation*, The University of Michigan, Ann Arbor, USA.

Lopez-Almansa F, Yazgan AU and Benavent-Climent A (2013), "Design Energy Input Spectra for High Seismicity Regions Based on Turkish Registers," *Bulletin of Earthquake Engineering*, **11**(4): 885–912.

Okur A and Erberik MA (2012), "Adaptation of Energy Principles in Seismic Design of Turkish RC Frame Structures. Part I: Input Energy Spectrum," *Proceedings of the 15th World Conference on Earthquake Engineering*, Lizbon, Portugal.

Park HG and Eom TS (2006), "A Simplified Method for Estimating the Amount of Energy Dissipated by Flexure Dominated Reinforced Concrete Members for Moderate Cyclic Deformations," *Earthquake Spectra*, **22**(3): 459–490.

Pettinga JD and Priestley MJN (2007), "Accounting for P-Delta Effects in Structures When Using Direct Displacement-Based Design," *Research Report ROSE-*

2007/02, European School for Advanced Studies in Reduction of Seismic Risk, IUSS Press, Pavia, Italy.

Pettinga JD and Priestley MJN (2008), "Accounting for P-Delta Effects in Structures When Using Direct Displacement-Based Design," *The 14th World Conference on Earthquake Engineering*, Beijing, China.

PEER (2016), Pacific Earthquake Engineering Research Center Strong Ground Motion Database, http://ngawest2.berkeley.edu/.

Priestley MJN (2003), "Myths and Fallacies in Earthquake Engineering, Revisited," *The Ninth Mallet Milne Lecture*, European School for Advanced Studies in Reduction of Seismic Risk, Rose School, Pavia, Italy.

Priestley MJN, Calvi GM and Kowalsky MJ (2007), *Displacement-Based Seismic Design of Structures*, IUSS Press, Pavia, Italy.

Rodrigues H, Varum H, Arêde A and Costa A (2012), "A Comparative Analysis of Energy Dissipation and Equivalent Viscous Damping of RC Columns Subjected to Uniaxial and Biaxial Loading," *Engineering Structures*, **35**: 149–164.

SAP2000 Ultimate (2016), *Integrated Solution for Structural Analysis and Design*, Computers and Structures Inc. (CSI), Berkeley, California, USA.

SeismoSpect (2016), Seismosoft, Earthquake Engineering Software Solutions, Pavia, Italy.

Tselentis GA, Danciu L and Sokos E (2010), "Probabilistic Seismic Hazard Assessment in Greece – Part 2: Acceleration Response Spectra and Elastic Input Energy Spectra," *Natural Hazards and Earth System Sciences*, **10**(1): 41–49.

TSDC (2007), *Turkish Seismic Design Code*, Ministry of Public Works and Settlement, Ankara, Turkey.

TS500 (2000), *Requirements for Design and Construction of Reinforced Concrete Structures*, Turkish Standards Institution, Ankara, Turkey.

Uang CM and Bertero VV (1990), "Evaluation of Seismic Energy in Structures," *Earthquake Engineering & Structural Dynamics*, **19**(1): 77–90.

Wang F, Li HN and Yi TH (2015), "Energy Spectra of Constant Ductility Factors for Orthogonal Bidirectional Earthquake Excitations," *Advances in Structural Engineering*, **18**(11): 1887–1899.